Integrating mangroves in dike designs: effect of tree growth and failure

Alejandra Gijón Mancheño
a.gijonmancheno-1@tudelft.nl

Delft University of Technology
Vincent Vuik
HKV Consultants
Bregje (B.K.) van Wesenbeeck
Deltares
Bas (S.N.) Jonkman
Delft University of Technology
Rosanna van Hespen
Royal Netherlands Institute for Sea Research
Swarna Kazi
World Bank
Ignacio Urrutia
World Bank
Mathijs van Ledden
World Bank
Roelof (J.R.) Moll
Delft University of Technology

Article

Keywords:

Posted Date: October 27th, 2023

DOI: https://doi.org/10.21203/rs.3.rs-3458217/v1

Additional Declarations: No competing interests reported.

Version of Record: A version of this preprint was published at Scientific Reports on April 4th, 2024. See the published version at https://doi.org/10.1038/s41598-024-58705-4.

Integrating mangroves in dike designs: effect of tree growth and failure

A. Gijón Mancheño[1,*], V. Vuik[2], B.K. van Wesenbeeck[3], S.N. Jonkman[1], R. van Hespen[5], J.R. Moll[1], S. Kazi[4], I. Urrutia[4], and M. van Ledden[4]

[1]Delft University of Technology, Stevinweg 1, Delft, 2628CN, the Netherlands
[2]HKV Consultants, P.O. Box 2120, Lelystad, 8203AC, the Netherlands
[3]Department of Ecosystems and Sediment Dynamics, Deltares, P.O. Box 177, Delft, 2600MH, the Netherlands
[4]World Bank, 1818 H Street, 20433, Washington DC, USA
[5]Department of Estuarine and Delta Systems, WNIOZ Yerseke, Royal Netherlands Institute for Sea Research and Utrecht University, Netherlands
[*]a.gijonmancheno-1@tudelft.nl

ABSTRACT

Mangrove forests reduce wave attack along tropical coastlines, decreasing the design requirements of coastal embankments. Wave reduction by mangroves depends on their surface area and stability against storms, but both aspects are often oversimplified or neglected in coastal protection designs. Here we present a framework to evaluate how mangrove belts influence embankment designs, including mangrove growth and failure by overturning and trunk breakage. This methodology is applied to *Sonneratia apetala* mangroves seawards from embankments in Bangladesh, considering forest widths between 10-1000 m (cross-shore). For design water levels of 5 m, wave reduction by mangrove forests shorter than 1 km mostly affects the slope protection and the bank erodibility, whereas the embankment height is less influenced by mangroves. *Sonneratia apetala* trees induce a relative maximum in wave attenuation by 10 years old, due to their large submerged canopy area. Once trees grow older than 20 years old, their canopy is emergent, and most wave attenuation is caused by trunk and roots. Canopy emergence exposes mangroves to wind loads, which are much larger than wave loads, and can cause tree failure during cyclones. These results stress the importance of including tree surface area and stability models when predicting coastal protection by mangroves.

Introduction

Mangrove forests are tropical coastal ecosystems that reduce flood risk along coastlines worldwide[1–4], among many other ecosystem services[5]. Wave and surge attenuation by mangroves is estimated to reduce flood protection costs by 65 billion USD per year[2], and could decrease the adaptation costs of coastal infrastructure by 71-168 billion USD by 2080[4]. Besides those benefits, mangroves can counteract up to 7 mm/year of sea level rise by trapping sediment[6,7] and building up peat[8], and they sequestrate carbon and mitigate global warming[9]. Mangroves are thus being increasingly included in coastal protection plans, and specifically on the design of coastal embankments. Nevertheless, existing studies of flood mitigation by mangroves[2–4] highly simplify the vegetation characteristics and assume constant plant properties worldwide, both over time and space. This can introduce large inaccuracies in predictions of flood risk reduction by mangroves, as there are many different species across the globe, with very different geometries[10] and present at varying tidal elevations[11–14]. Moreover, mangrove forests can be damaged during extreme events[15,16], while existing studies of flood risk reduction by mangroves often neglect vegetation failure and its effect on coastal protection.

In this paper we present a method to predict the effect of tree geometry on the coastal protection provided by a mangrove belt, assessing whether the vegetation is likely to fail, and evaluating how the presence of a forest influences dike designs during the lifetime of trees. The method is applied to the coastal system of Bangladesh, since this country has large vulnerability to coastal flooding[17] and large mangrove potential[18,19]. Bangladesh is exposed to frequent cyclones, which induce water levels of up to 13 m, and has a large population living in low-lying areas[17,20]. Its coastal system is therefore defended by a system of 6000 km of peripheral embankments that enclose 139 polders. As the embankment system is being upgraded to provide sufficient safety against rising water levels, integration of mangroves into embankment designs could reduce the design requirements of the structures[2–4,21–23], besides giving additional resilience against climate change[9], enhancing the local biodiversity[24], and increasing the water quality[25] among other benefits[5]. Short mangrove fringes (< 1 km) are likely to have a small effect on surge levels, since observed attenuation rates at other countries showed surge reductions of 0-0.20 m per km of forest[26,27], and modelling studies in Bangladesh support those observations[28]. However, mangroves can significantly attenuate short waves, between 5-100% for a fringe of 100 m (from sea to land)[29–32], which would reduce the the wave loads on coastal embankments.

The effect of mangroves on the embankments is here quantified with a wave attenuation model based on that of Mendez and Losada[33], and by using the attenuated waves as an input of the embankment design formulas. Wave energy attenuation by mangroves is calculated by integrating the wave energy dissipation caused by the trees and removing this energy loss from the wave energy balance. The energy dissipation is integrated numerically over the vertical, considering a tree structure that changes over the vertical coordinate. The frontal area of *Sonneratia apetala* is obtained from the analysis of field pictures. Changes in vegetation geometry over time are modelled using empirical expressions for tree growth from the literature[34,35]. The potential failure of the trees by either overturning or trunk breakage is estimated by comparing moment due to the forces induced by wind and waves with the resisting moment of the vegetation[36,37]. Finally, the calculated wave heights are used as an input in the design formulas of embankments[38–40] to evaluate how the presence of a mangrove belt would influence their height, slope protection needs, and the wave-driven shear stresses at their toe.

Theoretical Background

Mangrove geometry

Wave attenuation by a mangrove forest varies with tree geometry and relative ground elevation with respect to the tidal levels. Mangroves inhabit sheltered coastal areas above mean sea level and below mean high water, where different species usually distribute along shore-parallel bands depending on their propagule dispersal[41], and on the flooding limits that they can endure, among other factors[42]. In Bangladesh the mangrove pioneer species with more planting success are *Avicennia officinalis* (Baen) and *Sonneratia apetala* (Keora), with *S. apetala* being the most planted out of the two[18].

When mangroves colonize a new site, their wave reduction efficiency rises as they grow their trunk[43], and develop their root[43] and branch system. Their growth rate is influenced by multiple biophysical parameters, like soil composition[44], water salinity[45], or temperature[46]. Differences in growth between sites are illustrated in Figure 1 for *S. apetala* mangroves in Bangladesh[34,35] and China[47]. Mangrove plantations with less than 20 years old show similar trunk diameters in both countries (Figure 1, b-c), but for older ages, Bangladeshi mangroves grow taller at the sites compared in Figure 1 b-c. The larger size of Bangladeshi trees could be caused by a more suitable habitat (e.g., a more favourable climate), given that *S. apetala* is native of the Sundarbans and was imported into China during the 80s[48], but local differences between sites could also explain variations in growth.

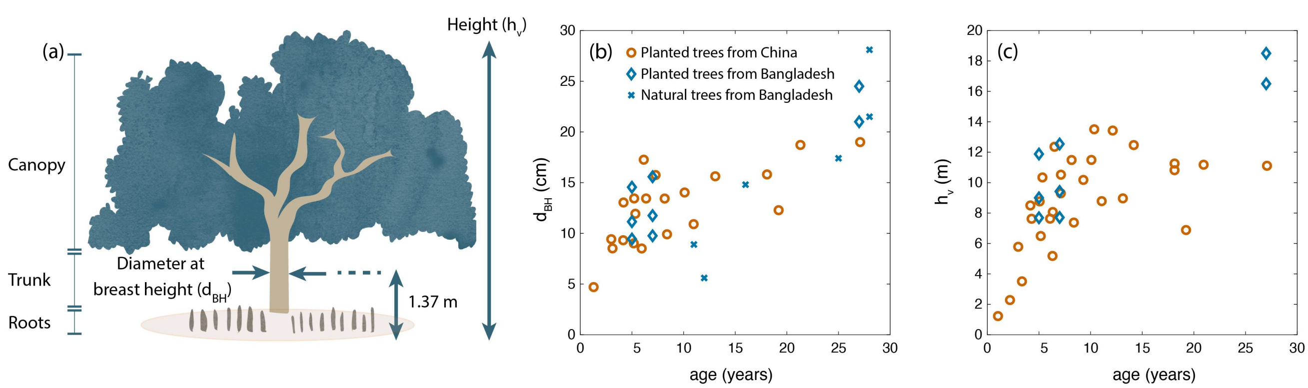

Figure 1. (a) Parts of a *Sonneratia apetala* mangrove, including canopy (formed by leaves and branches), trunk, and pneumatophore roots. (b-c) *S. apetala* size as a function of tree age for natural forest stands in Bangladesh[45] and for planted trees in Bangladesh[34,35] and China[47]. Plot (b) presents the trunk growth, represented by the diameter at breast height d_{BH} (cm), and plot (c) displays changes in tree height h_v (m), from Gijón Mancheño et al.[49]

Although the data in Figure 1 provides an indication of how the trunk diameter and tree height change as *S. apetala* trees grow, while Table 1 gives an impression of the relationship between root characteristics and tree height, the evolution of the total frontal area of *S. apetala* mangroves with age has not been measured in the field. For other mangrove species, the equivalent canopy width has been defined using several approaches, like assuming that the width of the canopy is given by the outer contour of the tree crown including[50] or neglecting[29,30] voids and empty areas. Other studies express the canopy area as a field of cylinders[51], but without basing the canopy area on field measurements of the total branch area. Lastly, some authors

Table 1. *S. apetala* mangrove characteristics from field studies, based on Gijón Mancheño et al.[49] The table lists study authors, country, and mangrove characteristics: pneumatophore height (h_r, in cm), pneumatophore diameter (d_r, in cm) pneumatophore density (N_r, pneumatophores per m^2), mangrove trunk diameter at breast height d_{BH} (cm), mangrove height (h_v, in m), mangrove density (N_v, mangroves per m^2), and mangrove age in years.

Author	Country	h_r [cm]	d_r [cm]	N_r [roots/m^2]	d_{BH} [cm]	h_v [m]	N_v [trees/m^2]	Age [yr]
Chen et al. (2021)	China	8	-	-	7	2.3	0.01	2
Duan et al. (2021)	China	18	0.8	-	35	14.8	0.17	-
Zhang et al. (2019)	China	12	-	253	-	18.3	0.17	-
Mazda et al. (2005)	Vietnam	14	0.7	131	12	-	-	
Dasgupta et al. (2017)	Bangladesh	104	15	-	51	-	0.01-0.04	-

neglect canopy leaves and branches, and assume that the tree area above the root system is given by the area of the trunk[52].

Using the full canopy volume in wave calculations would overestimate the obstruction exerted by the trees, as part of the canopy is porous to the flow. Since leaves were found to have a small effect on wave attenuation for willow trees due to their high flexibility[53], and they can also be pulled by wind and waves[37], including the full leaf area in b_v predictions most likely overpredicts the effect of trees during extreme events. For willow trees, tree trunk and branch models were developed by Kalloe et al.[54] and successfully used to predict wave attenuation measurements by van Wesenbeeck et al.[53] Models for the growth of the trunk and root system of *Rhizophora sp.* have also been developed by Maza et al.[43] However, geometry models are not available for the pioneer species in Bangladesh.

Mangrove stability against storms

Mangroves can protect the coast from storm events but they can also be degraded by the impact of winds and waves. Hurricanes and cyclones can directly damage mangroves by defoliating them, by breaking their trunk or branches, or by overturning them[55–57]. Extreme events can also damage mangroves by altering their habitat, for instance, by changing the local salinity, hydrology, topography, sediment conditions, or the forest structure[58]. In Bangladesh the cyclone Sidr (2007) damaged between 11%[15] and 45%[16] of the total area of the Sundarbans. Large-scale cyclone damage in the Sundarbans (where more than 5% of the forest is affected) is estimated for wind speeds exceeding 100 km/h[59], based on observations of past cyclones. This order of magnitude is also consistent with records of forest damage in Florida[56], which indicated that few trees are broken or tipped up for wind speeds between 119-153 km/h. However, the cyclone Reshmi (with wind speeds between 46-86 km/h) locally caused structural damages over >60% at coastal areas along the cyclone eyepath, even though the total damage at the scale of the Sundarbans was small[57,60]. Mangroves can recover over time[15] but landward areas may be vulnerable to storm damages while the vegetation is recuperating[61]. Predicting mangrove degradation due to cyclones is thus necessary to assess the long-term forest resilience, but this step is hindered by the absence of mangrove stability models.

Trunk breakage and tree overturning have been investigated for pines, cedars, and other terrestrial trees under the action of wind loads[62]. When mangroves are submerged during storms, wave forces could also destabilize trees. The importance of waves versus wind is probably a function of tree submergence, with wave loads being more dominant for rising water levels. However, since mature *S. apetala* mangroves can grow up to 24 m in height[63], and 3-5 m surge heights are common in Bangladesh[64,65], a considerable proportion of the surface area of mangroves will be pushed by the wind during cyclones. Previous studies have investigated the stability thresholds for mangrove seedlings[66], and compiled observations of mangrove failure during hurricanes[56,57,59,60,67], but predictive models for mangrove stability against winds and waves are still lacking.

Model development

The methodology to incorporate mangroves belts in the design of coastal embankments is illustrated in Figure 2. This method comprises: (1) a wave propagation model, (2) an assessment of potential vegetation failure due to wave and wind loads, and (3) the calculation of the embankment design.

Wave transformation

Cross-shore wave transformation is computed from the wave energy balance[33]:

$$\frac{\partial E c_g \cos\theta}{\partial x} = -\varepsilon_b - \varepsilon_v \tag{1}$$

where E is the wave energy per unit area (J/m^2), c_g is the group celerity (m/s), θ is the mean wave direction (rad), D_w represents wave dissipation due to depth-induced breaking (W/m^2), and D_v represents wave dissipation by mangrove trees (W/m^2). Here

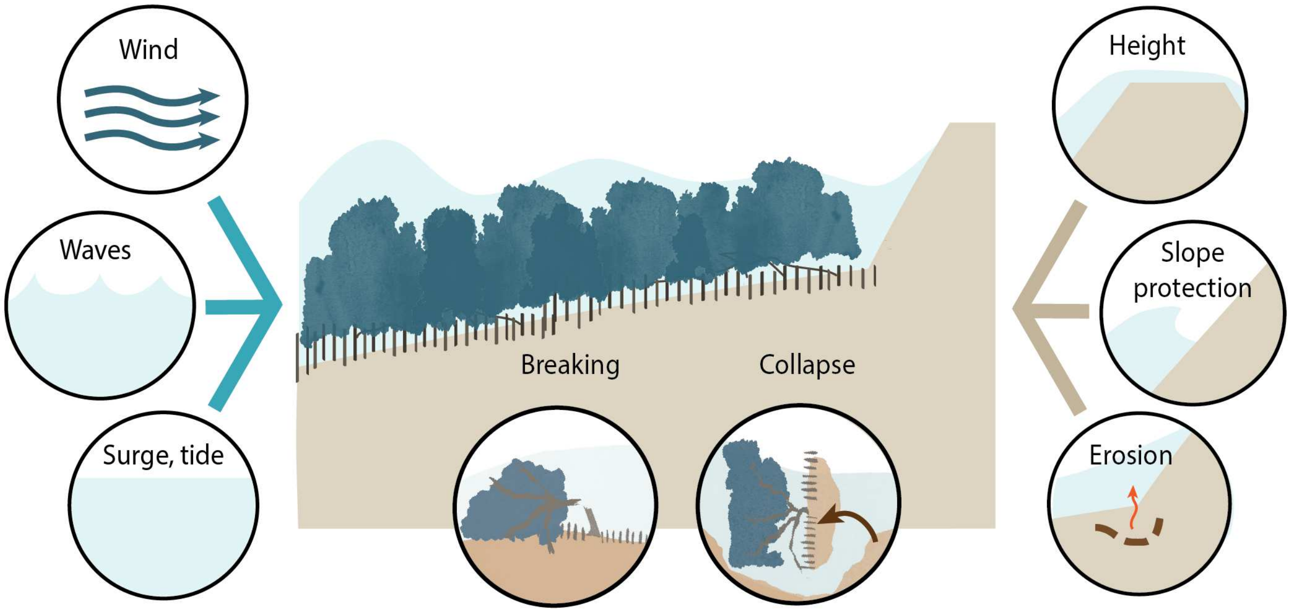

Figure 2. Illustration of the method to integrate mangroves in the design of coastal embankments, modified from Gijón Mancheño et al.[49]. This methodology has several steps: (1) reducing wave attack due to the presence of a mangrove belt as a function of the local surge level and wave height, (2) assessment of tree stability against waves and winds, and (3) calculation of embankment design (considering wave attenuation by the trees), specifically the structure crest height, size of slope revetment blocks, and erodibility of the embankment toe.

we have assumed that wave dissipation by bed friction is an order of magnitude smaller than the energy loss due to wave breaking or due wave dissipation by the vegetation[33]. Equation 1 is solved using a forward stepping scheme from the offshore boundary towards the land over cells of size Δx and constant water depth, as done by Mendez and Losada[33].
Wave dissipation due to depth-induced breaking is computed using the formulation of Thornton and Guza[68]:

$$\varepsilon_b = \frac{3\sqrt{\pi}}{16}\rho g \frac{B^3 f_p}{\gamma_{br}^4 h^5} H_{rms}^7 \tag{2}$$

Where f_p is the peak frequency (s^{-1}), and B (-) and γ_{br} (-) are empirical coefficients that are set to the default values used by Mendez and Losada[33]: $B = 1$ and $\gamma_b = 0.6$.
Wave dissipation by the mangrove vegetation is modelled as the work of the hydrodynamic forces acting on the trees. The wave load acting on each tree is estimated using the formulation for hydrodynamic forces acting on cylinders of Morison et al.[69]:

$$F_w = \int_0^{h_v} \left(\frac{1}{2}\rho_w c_{D,w} d u_w(z)|u_w(z)| + \rho c_M \frac{\pi d^2}{4}\frac{\partial u_w}{\partial t} \right) \partial z, \tag{3}$$

where ρ_w is the water density (kg/m^3), $c_{D,w}$ and c_M are the bulk drag and inertia coefficients under waves (-), d is the diameter of the cylinder (m), $u_w(z)$ is the wave-driven velocity at a height z from the ground from linear wave theory (m/s), h_v is the tree height (m), and η is the water surface elevation (m). Large-scale experiments with willow trees provided values of $c_{D,w} = 0.7 - 2$, which is also consistent with the expected drag range for cylinder fields with porosities above 0.6[70]. For circular cylinders, $c_M = 0 - 2$[69].

The depth-integrated and time-averaged work over a forest is calculated as:

$$\varepsilon_v = \frac{1}{T_p}\overline{\int_0^{h_v} \frac{1}{2}\rho_w c_{D,w} b_v(z) N_v u_w(z)^3 dz dt} \tag{4}$$

where T_p is the peak wave period (s), t is the time (s), b_v is the integrated tree width at an elevation z from the ground (m), and N_v is the tree density per unit area (trees/m^2). Equation 4 is integrated numerically over the vertical coordinate over cells with a size Δz and varying width $b_v(z)$.

Validation of wave model

The model predictions of wave attenuation are validated for several scenarios: (1) an unvegetated profile, (2) a vegetated profile where plant properties are constant over the vertical but vary along the profile, and (3) a vegetated profile where plant properties vary over the vertical but remain constant along the profile. These different cases are modelled to ensure that the modules of wave breaking (Equation 2) and wave dissipation by vegetation (Equation 4) are well implemented, and to validate both the horizontal (Equation 1) and vertical (Equation 4) integration of the energy dissipation terms.

The first two situations are tested against the results of Vuik et al.[21], who measured wave propagation through a salt marsh fringe and modelled it using SWAN. Wave transformation through the salt marshes is modelled for a significant wave height of $H_{m0} = 0.6$ m and a peak period of $T_p = 3.5$ s at the offshore boundary. The bathymetry varies between an offshore water depth of 2 m, and a nearshore water depth of 0.5 m. The salt marshes extend over a (cross-shore) width of 55 m and have uniform properties over the vertical coordinate and varying vegetation properties across the profile, with h_v = 0.2-0.3 m, b_v = 2.7-3 mm and N_v = 944-1520 plants/m^2. A drag coefficient of $c_{D,w} = 0.4$ is used in the simulations, which is equal to the value calibrated by Vuik et al.[21] The model output shows good agreement with the results of Vuik et al.[21] at all cross-shore locations, with and without vegetation (Figure 3).

In the third situation, with vegetation properties changing over the vertical, the model is tested for the conditions of the large-scale flume experiments with pollarded willows of van Wesenbeeck et al.[53], where waves travelled across 32 willow trees with a height of 6 m, and a total forest length of 40 m. This study is selected as it is the only large-scale wave experiment with real trees during extreme conditions that provides high-resolution information of the tree canopy, measured with terrestrial laser scanners. Offshore wave heights (at the wave maker), wave periods, and water depths (at the location of the trees) reached values of $H_{m0} = 0.4 - 1.4$ m, $T_p = 2.8 - 6.7$ s, and $h = 3 - 4.5$, respectively. The vertical distribution of the tree surface area was quantified by Kalloe et al.[54], who measured vegetation parameters varying between b_v = 0.03-0.3 m over the tree height, for trees placed with a density of N_v = 1 tree/m^2. The input drag coefficients for the validation cases were obtained from van Wesenbeeck et al.[53] and range between $c_{D,w} = 1.02 - 1.87$. The modelled wave decay through the forest also agrees with the measurements by van Wesenbeeck et al.[53], as illustrated in Figure 3b.

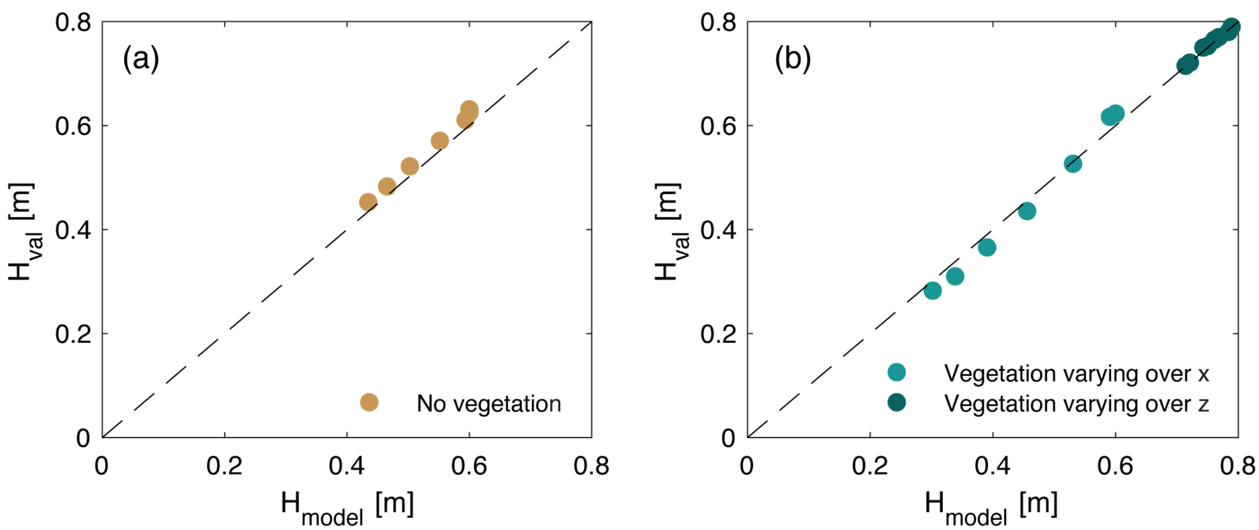

Figure 3. Comparison between wave heights obtained using the wave model given by Equations 1-4, H_{model}, and the validation wave heights H_{val} from (a) model results obtained with an unvegetated profile by Vuik et al.[21], and (b) case studies with vegetation from Wesenbeeck et al.[53] (dark green dots) and Vuik et al.[21] (light green dots).

Mangrove failure

Wind loads

The wind forces acting on a mangrove tree are estimated with a quadratic (form) drag equation:

$$F_a = \int_0^{h_v} \frac{1}{2}\rho_a c_{D,c} b_v(z) G u_a(z)^2 dz \tag{5}$$

Where ρ_a is the air density (kg/m^3), $c_{D,c}$ (-) is the drag coefficient for wind flows, which varied between 0.2-1 in wind tunnel experiments with terrestrial trees[71], with lower $c_{D,c}$ values corresponding with higher tree deflection and higher values representing small tree motion, G is an empirical gust factor that is given a value of 1.2 for high wind speeds[72] (-), and u_a is the maximum sustained wind speed relative to the tree motion (m/s), measured at 10 m from the ground and averaged over a period of 1-3 minutes. Above the vegetation, the wind speed is often assumed to follow a logarithmic velocity profile over the vertical coordinate z[62]:

$$u_a(z) = \frac{u_a^*}{k} ln \frac{z}{z_0} \tag{6}$$

Where z_0 is the roughness height (m), which can reach values of the order of 0.0002 m for water, 0.02 m for unvegetated sites[72], and up to 5 m for tall forests[62], u_a^* is the friction velocity (m/s), and k is the von Karman constant (-), equal to 0.4.

Moment caused by waves and wind

The potential for tree failure is calculated using the overturning moment acting on the tree:

$$M = \int_0^{h_v} dF(z) z dz \tag{7}$$

where the force for each segment will be equal to the wind driven force (Equation 5) above the water surface, and to the wave-driven force (Equation 3) below water.

Resisting moment to breakage

Trunk breakage is estimated by comparing the overturning moment experienced by the tree M (Equation 7) with the maximum bending moment that a tree can withstand without breaking, M_{break}[36]:

$$M_{break} = \frac{\pi}{32} f_{knot} \sigma_u d_{BH}^3 \tag{8}$$

Where σ_u is the modulus of rupture of the wood tissue (N/m^2), d_{BH} is the trunk diameter at breast height (m), and f_{knot} is a factor that reduces the wood strength due to the presence of knots (-), usually between $f_{knot} = 0.8 - 1$.

Resisting moment to toppling over

Tree failure by toppling over can also be estimated by comparing the bending moment acting on the tree with the critical overturning moment M_{over}, measured in tree pulling experiments[73]:

$$M_{over} = C_r W \tag{9}$$

Where C_r is a dimensional regression constant varying between $C_r = 60 - 200$ m^2/s^2, and W is the tree trunk weight in kg.

Evaluation of mangrove failure model

To evaluate the model predictions of mangrove stability (Equations 7-9), since we could not find observational studies of *S. apetala* tree failure that provided all required modelling variables at one site (e.g., local wind speed, water level, vegetation damage, vegetation properties and soil characteristics), we have conducted a semi-quantitative verification of the tree failure model gathering information from several studies to define the necessary modelling parameters. This section thus shows the relative behaviour of the model for different tree sizes and wind conditions, but it is recommended to collect tree failure data by monitoring mangrove forests (e.g., installing wind stations and pressure sensors that can measure over several months and/or years) and conducting detailed surveys (including spatial variations in vegetation, soil properties, and hydrodynamic conditions) before and after storm seasons, to further test and develop tree failure models.

The case studies used to evaluate the tree failure model for *S. apetala* are the cyclone Sidr (2007) in Bangladesh, and the thyphoon Mangkhut (2018) in China. In the Sundarbans (Bangladesh), *S. apetala* trees with heights above 15 m were broken during cyclone Sidr (2007)[74]. The location of the damaged trees was not specified, but mangrove species maps show that *S. apetala* trees are mostly present along the south east of the Sundarbans[75], where surge levels reached varied 2-6 m during Sidr (2007)[76,77], and where 1-min sustained wind speeds varied between 60-180 km/h[78]. In Honghai wan (China), 6-m tall *S. apetala* planted mangroves were able to stay intact during thyphoon Mangkhut (2018) with water levels up to 3 m in the mangrove forest[79]. The typhoon landed 200 km away from the mangrove site with maximum 2-minute sustained winds of 160 km/h, whereas at the nearby city of Shanwei (13 km away from the mangrove plantation), fallen trees, traffic accidents, and damaged advertisement boards were reported[79]. Such wind damages approximately correspond with Beaufort scales 9-10, and with wind speeds between 75-102 km/h.

To estimate the forces acting on the trees during cyclone Sidr (2007) and thyphoon Mangkhut (2018), we assume depth-limited waves in shallow water, and that tree swaying takes place during cyclonic conditions (and thus $c_{D,w} = 0.7$, based on large-scale wave experiments with natural willow trees, and $c_{D,c} = 0.2$ based on wind tunnel experiments with western red cedars[71]). The forces are calculated at the edge of the forest (neglecting canopy effects), and we assume $f_{knot} = 1$ in tree stability calculations. The surface area of *S. apetala* trees is estimated using the model of the Methods section and their tree weight using the biomass allometric relationships of Zhu et al.[80] Mangrove stability is calculated using the full range for the empirical coefficient for overturning ($C_r = 60 - 200$ m^2/s^2[73]), since there is no specific information of C_r values for mangroves, and using the expected range of modulus of rupture for *S. apetala* (σ_u = 37±7 N/mm^2)[37].

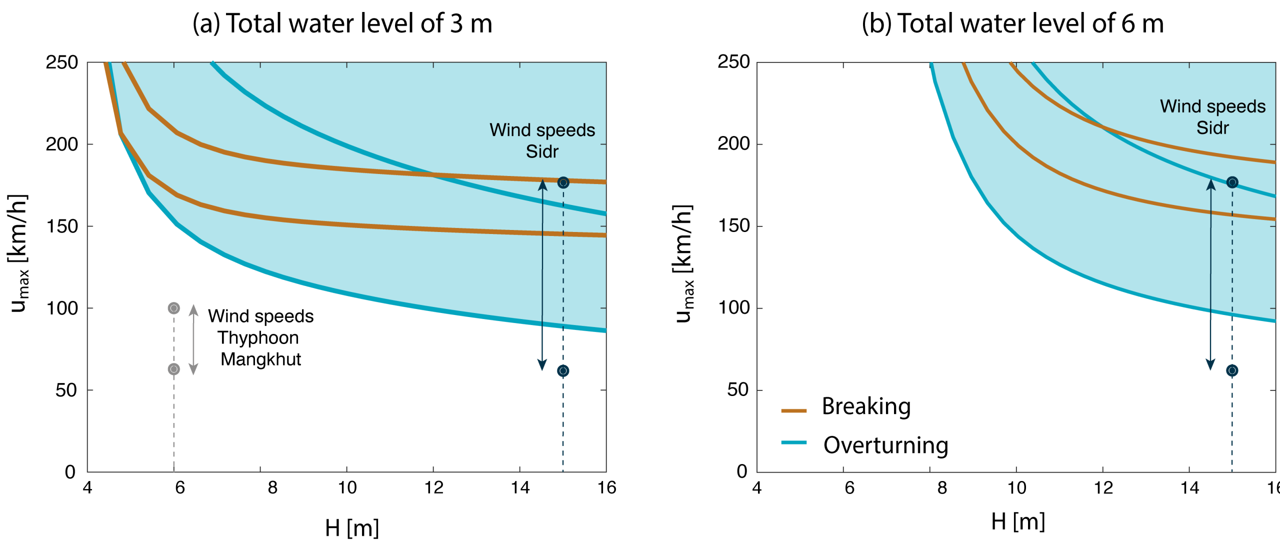

Figure 4. Maximum wind speed that mangroves can withstand without failing (u_{max}) as a function of tree height (H). The white region of the plots correspond with combinations of wind speed and tree height for which there is no failure, whereas the areas filled in blue are the combinations for which failure occurs. The maximum wind speed for overturning is shown by blue lines, and the maximum wind speed for trunk breaking by brown lines. The lower and upper blue lines correspond with the minimum and maximum value of the empirical coefficient for overturning for terrestrial trees[73], and for the brown lines with the minimum and maximum value for the modulus of rupture of *S. apetala* trees[37]. Plot (a) shows model results with a total water level (with respect to MHW, including tide) of 3 m, and (b) shows results obtained with a total water level of 6 m.

For the conditions expected during Thyphoon Mangkhut, model results show no damage for tree heights of 6 m (Figure 4, a). The planted mangroves did not topple over, probably because they were part of a 6-year-old plantation with relatively short trees (Figure 1). Failure could have occurred to trees with more than 10 m in height, or for 6-m tall trees if the cyclone had been closer to the mangrove forest and caused stronger local winds. It should be noted that the sustained wind speeds of Figure 4 are multiplied by a gust factor to estimate the drag forces (factor G in Equation 5), since gusts are large determinants of tree failure[81].

The local water level was not reported at mangrove sites damaged by Sidr (2007), and we therefore model two possible water levels (Figure 4 a-b), to evaluate what would happen for the expected range of maximum wind speeds. Model results support that the relative timing between surge level and wind speed largely influences mangrove failure. High water levels shelter mangroves from the wind, specially for young individuals. For instance, 15-m tall *S. apetala* trees would fail under winds of under winds of 90-180 km/h with a surge level of 3 m (Figure 4, a), but could withstand stronger winds, between 96-180 km/h, with a surge level of 6 m (Figure 4, b). Model results thus agree with the observation that failure can occur for 15-m tall trees under most of the wind range experienced during Sidr (2007), however, more detailed measurements are recommended for a precise model validation, and to narrow down the range of C_r for mangroves.

Effect of mangroves on dike design

Embankment height

The height of an embankment is usually chosen in such a way that the overtopping discharge remains below a critical threshold, which depends on the erosion resistance of the crest and inner slope of the embankment. Mangroves reduce the value of H_{m0} at the structure, and thus decrease the overtopping discharge for a given design. The expected value of the overtopping discharge over a sloping embankment q can be calculated using the formula of EurOtop[38]:

$$q = \sqrt{gH_{m0}^3}\frac{f_1}{tan(\alpha)}\gamma_b \varepsilon_{m-1.0} e^{-\left(f_2 \frac{h_{crest}-h}{\varepsilon_{m-1.0} H_{m0}\gamma_b\gamma_f\gamma_\beta\gamma_v}\right)^{f_3}} \tag{10}$$

where q is the overtopping discharge per meter (m^3/m/s), g is the gravitational acceleration (g = 9.8 m/s^2), H_{m0} is the spectral wave height (m), f_1 is an empirical factor equal to 0.026 (-), α is the angle of the outer slope (-), $\xi_{m-1.0}$ is the breaker parameter (-), γ_b is the influence factor for a berm (-), γ_f is the influence factor for roughness elements on the slope (-), γ_β is the influence factor for oblique wave attack (-), γ_v is the influence factor for vertical wall (-), f_2 is an empirical factor equal to 2.5 (-), h_{crest} is the crest level (m), h is water level (m), and f_3 is an empirical factor equal to 1.3 (-).

Slope protection

Wave attenuation by mangroves can also reduce the stone weight required to protect the embankment slope. The slope protection of the embankment can be calculated with the expression of Pilarczyk[39,40].

$$\frac{H_{m0}}{\Delta D} = \frac{F\cos\alpha}{\varepsilon_{m-1.0}^b} \tag{11}$$

Where H_{m0} is the spectral significant wave height at the toe of the structure (m), D is the thickness of the cover layer (m), Δ is the relative density of concrete with respect to water (-), F is a stability factor between 3-6 for a revetment formed by concrete blocks (-), and b is an exponent equal to 0.67 for semi-permeable block revetments (-).

Erosion at the toe

Wave attenuation by mangroves reduces the shear stresses acting at the toe of the embankment, and hence decreases the erosion rates. The effect of wave attenuation by mangroves on the shear stresses (τ_w) acting on the embankment toe can be calculated according to Equation 12:

$$\tau_{b,w} = \frac{1}{4}\rho_w f_w u_{rms}|u_{rms}| \tag{12}$$

where u_{rms} is the orbital velocity associated to the root mean wave height, f_w is the wave friction factor, defined as[82]:

$$f_w = min\left(\exp\left(-6+5.2\left(\frac{u_{rms}}{2.5d_{n50}\omega_m}\right)^{-0.19}\right), 0.3\right) \tag{13}$$

with d_{n50} being the mean grain size (m) and ω_m the mean wave frequency (rad/s).

Modelling scenarios

The design wave height and water level at the potential afforestation sites (see Figure 7 of Gijon Mancheno et al.[19]) are $h =$ 4.5-5 m and $H_{m0} =$ 2-3 m[83], respectively, corresponding with a 25-year safety standard, including +1 m in the water levels due to sea level rise (equivalent to a worst case scenario for 2050 and an average case for 2100). The report of IWM[83] does not specify the wave period associated to the wave height but assumes a wave steepness of $s_0 = 0.05$, where the steepness s_0 is defined as the ratio between the wave height H_{m0} and the wavelength L. We also use this steepness for the wave attenuation calculations, as we aim to test the effect of mangroves on the design condition of the structures. The corresponding wavelength is obtained as $L = s_0/H_{m0}$, and the wave period is derived using the dispersion relation for linear wave theory with the design water level. For the bathymetry, schematized linear profiles with slopes between $0.001-0.1$ are considered, and the embankment toe is set at an elevation equal to mean high water (MHW).

Wave attenuation across the profile is modelled for forest (cross-shore) widths between 10-1000 m (seawards from the MHW point), and forest ages between 1-50 years old. Equations 1-4 are solved with a cross-shore grid size of Δx = 0.01 m and a vertical grid size of Δz = 0.005 m. The frontal area of the vegetation is described using the model presented in the Methods section, which is obtained combining empirical relationships for tree growth derived from Figure 1 with frontal areas obtained from field pictures (Figure 9). The vegetation density is set to $N_v = 0.1$ trees/m^2 (intermediate value in Table 1), ρ_w = 1030 kg/m^3, the drag coefficient is varied between $c_{D,w}$ = 0.7-2[53], and the inertia coefficient is given a value of c_M = 2[69]. For the wind loads, we assume that the mangroves are directly exposed to onshore winds (without canopy effects), ρ_a = 1.2 kg/m^3, the drag coefficient is varied between $c_{D,c}$ = 0.2-1[71], and the roughness height is set to z_0 = 0.0002 m[72] since we assess tree stability at the seawards edge of the forest. For the tree resistance against trunk breakage, the modulus of rupture of the wood tissue is varied within the range of σ_u = 37±7 N/mm^2 measured by van Hespen et al.[37], and f_{knot} = 1. For overturning calculations, the tree weight is estimated using the allometric relationships of Zhu et al.[80] and the regression constant C_r is varied between $C_r = 60 - 200$ m^2/s^2[73].

For the design of coastal embankments, we assume slopes of 1:8, armor layers (corresponding with $\gamma_f = 0.55$), and a berm (with $\gamma_b = 0.89$). We also assume perpendicular wave incidence (so $\gamma_\beta = 1$), and no vertical walls ($\gamma_v = 1$). In each scenario, the crest height of the embankment is adjusted to reach an overtopping rate of 5 l/m/s under design conditions, which is also used in the CEIP-1 design[84]. The size of the slope protection is calculated using Equation 11, with F = 3.5 (assuming a filter between the clay core and the outer concrete blocks) and b = 0.67. The shear stresses at the toe of an embankment are calculated assuming a grain size of $d_{n50} = 7\ \mu$m in Equations 12-13, corresponding to a muddy coastline.

Results and Discussion

Wave energy dissipation as function of forest age

The wave energy dissipation caused by the different parts of a mangrove tree (canopy, trunk, and roots) is shown as a function of tree age in Figure 5 (d). For the design water levels at the afforestation sites, the canopy causes most wave energy dissipation during the first 10 years, and has a significant role in wave dissipation until trees are 20 years old. Beyond that age, only trunk and roots contribute to wave dissipation since the canopy emerges from the water (see the submerged areas in Figure 5 c). Trunk and roots still continue to grow for trees older than 30 years old (Figure 1), and therefore wave dissipation continues to increase over time. Here we have extrapolated trunk growth rates measured in the field for trees with ages between 30-50 years old. Assuming no trunk and root growth beyond 30 years of age, the maximum dissipation would be 35 W/m^2 for a tree at the sea edge of the forest (12% smaller than the maximum value of Figure 5 d).

The wave height reduction produced by forests of varying widths is shown in Figure 5 (e-f). Wave attenuation is here defined as the reduction in wave height at the toe of an embankment (after waves have travelled through the forest) with respect to a situation without mangroves:

$$\frac{\Delta H}{H_{nv}}(\%) = 100\frac{H_{nv} - H_v}{H_{nv}} \tag{14}$$

where H_{nv} is the wave height at the embankment toe without mangrove vegetation (m), and H_v is the wave height at the same location considering the presence of a mangrove foreshore (m).

As observed in the wave dissipation rates, wave attenuation largely depends on tree age. Young trees below 2 years old induce attenuation rates smaller than 30% for all forest widths and wave attenuation increases as trees grow older. For a given age, wider forests increase the wave height reduction rates. For instance, extending the forest width from 100 m to 1000 m increases wave attenuation by a 50-year-old forest from 7% to 30% with $c_{D,w} = 0.7$ (Figure 5 e). These results are highly sensitive to the drag coefficient. The same forest widths would induce attenuation rates of 20% and 55% with $c_{D,w} = 2.0$ (Figure 5 f). The large sensitivity to $c_{D,w}$ suggest that good predictions of $c_{D,w}$, of the density N_v, and of the tree area are key for precise assessments of the effect of mangroves.

Existing studies investigating the effect of mangroves on coastal protection have focused on the description of the wave climate and used relatively simple descriptions of the geometry. However, the sensitivity analysis (Figure 6) suggests that the vegetation geometry is as important as the hydrodynamic conditions. For trees younger than 20 years old, since most of their surface area is at their canopy, the canopy height, canopy width and tree height are the most important geometrical parameters. For shorter species, like those of the Avicenniaceae family, the canopy could have a significant contribution for even longer periods (compared to *S. apetala*). For older *S. apetala* trees, whose canopy is above the water, the trunk diameter has the largest effect on waves.

Vegetation failure

The influence of wind and wave loads on tree stability is illustrated in Figure 7 (a). When trees are very young, they remain submerged during storm events and therefore experience wave loads (Figure 7 a). As mangroves grow (see Figure 5, c), they rise above the water surface and the emerged part of the tree is exposed to the wind. For partly submerged mangroves, wind loads are much larger than wave loads (Figure 7, b), since (1) the tree canopy constitutes a large part of the frontal area, and (2) because the (higher) wind speed causes relatively larger forces than the (lower) wave velocities, even if air has a lower density than water. This agrees with field observations by Myers and Lear[56], who observed that higher inundation levels sheltered trees from wind damage.

S. apetala trees younger than 10 years old can thus withstand strong winds without overturning for the embankment design conditions, as most of their frontal area is submerged and exposed to the relatively lower wave forces (Figure 7, c). As mangroves grow older they become heavier and more stable but wind forces act over a larger area and with a longer arm. The increase in overturning moment exceeds the increase in tree stability, and taller trees overturn under weaker winds (compared to

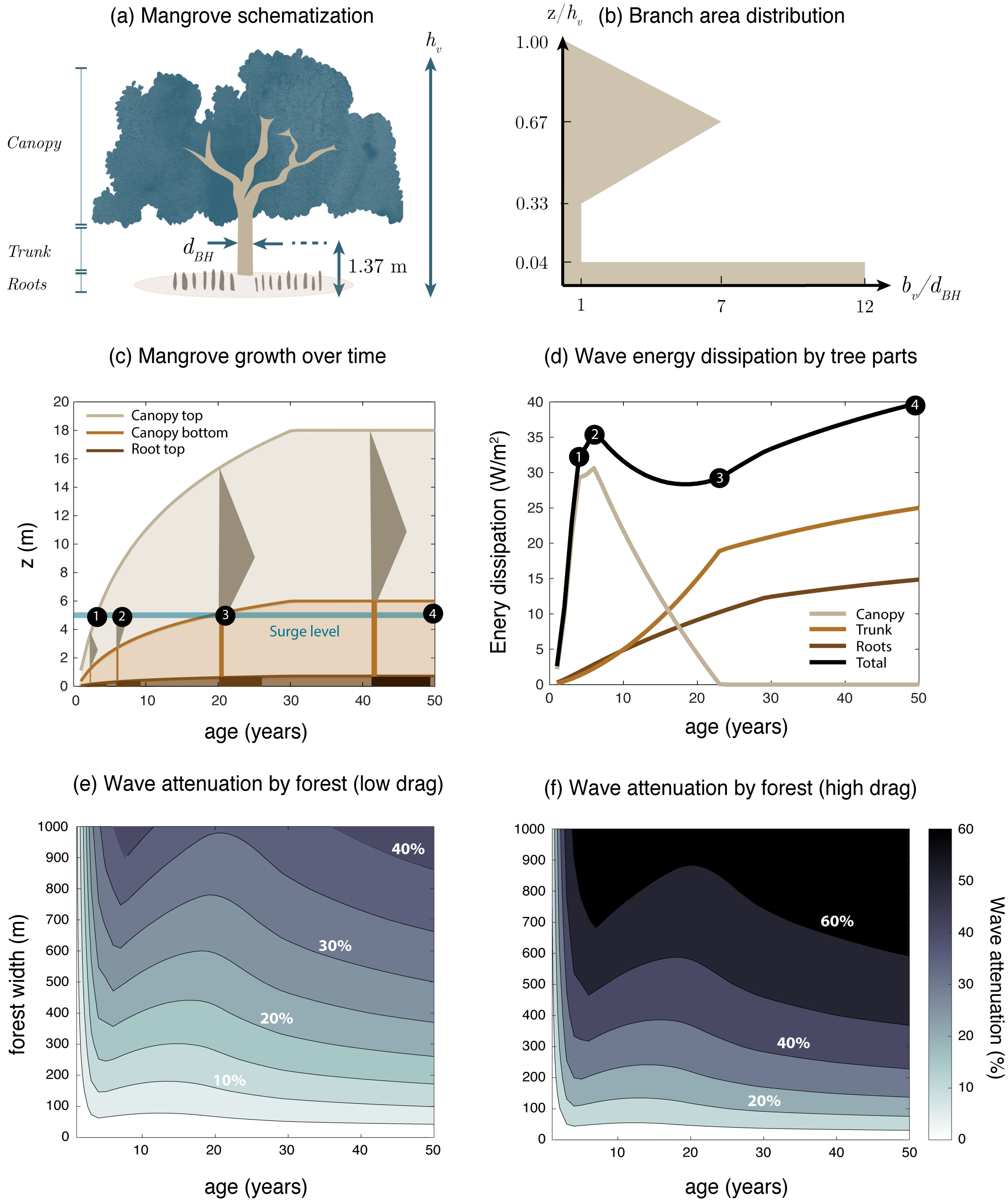

Figure 5. (a) Diagram illustrating the different sections of a tree: canopy, trunk, and roots. (b) The tree surface area of each section is parameterized as a function of the diameter at breast height (d_{BH}) and the tree height (h_v). The height of the different tree sections (calculated with the parameterizations of plot b) is shown as a function of tree age in (c), and the corresponding wave energy dissipation produced by mangroves at the seaward edge of a mangrove belt (D_v) in (d). The wave energy dissipation is calculated for an offshore wave height of $H_{m0} = 2$ m, and a water level of $h = 5$ m. The drag coefficient and the tree density are set to $c_{D,w} = 2$ and $N_v = 0.1$ trees/m^2, respectively. The wave attenuation for the same conditions but varying forest widths is shown in (e) for $c_{D,w} = 0.7$ and in (f) for $c_{D,w} = 2$.

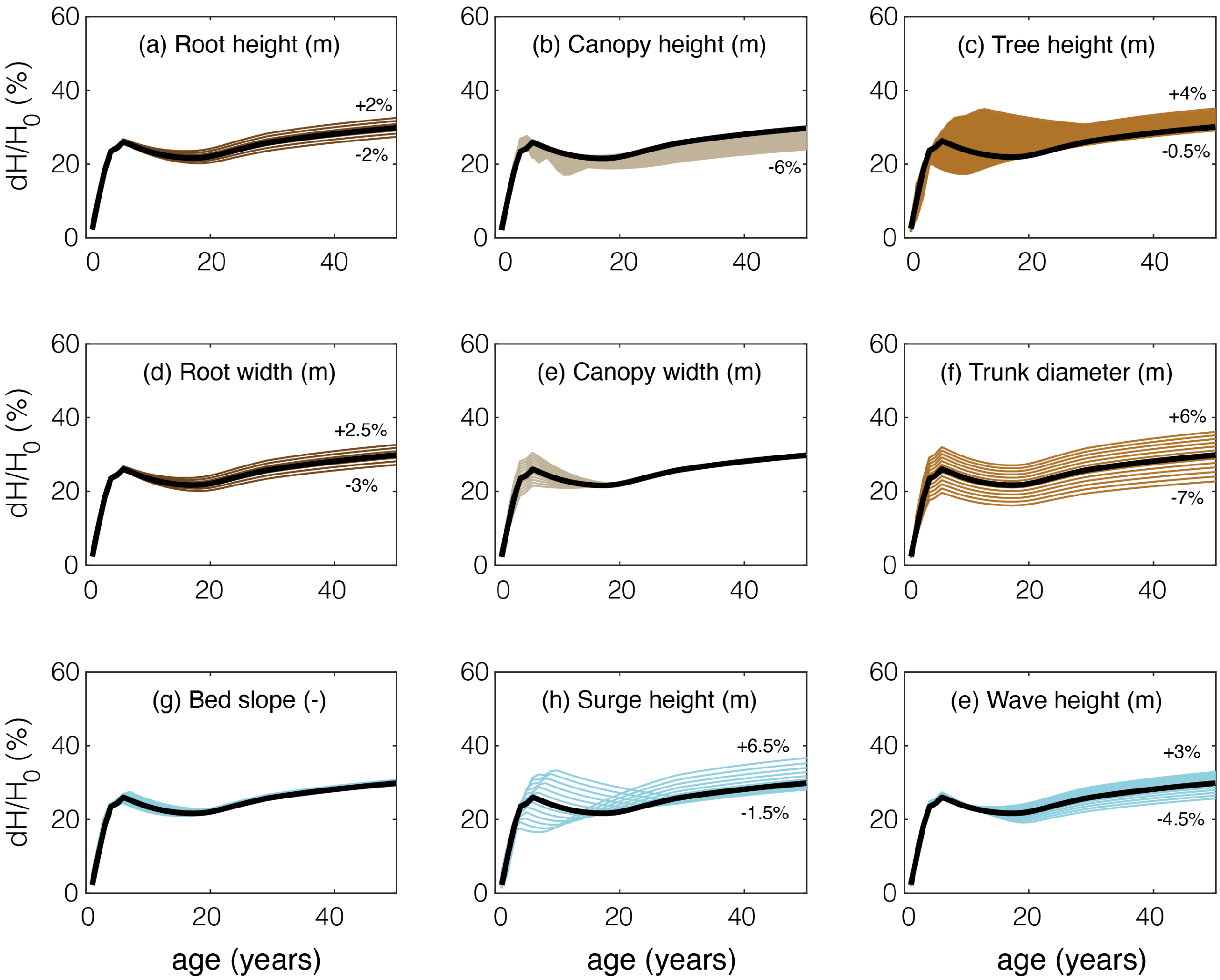

Figure 6. Sensitivity of wave attenuation to varying forest and hydrodynamic properties with respect to a reference scenario. The reference case is calculated with the geometrical tree model presented in Figure 5, $c_{D,w} = 2.0$, $N_v = 0.1$ trees/m^2, a forest width of 500 m, a slope of 1/1000, $H_{m0} = 2$ m and $h = 5$ m. The subplots show the variations in wave attenuation for changes between -30% and +30% of: (a) root height, (b) canopy height, (c) tree height, (d) root width, (e) canopy width, (f) trunk diameter at breast height, (g) bed slope, (h) surge height, (i) wave height.

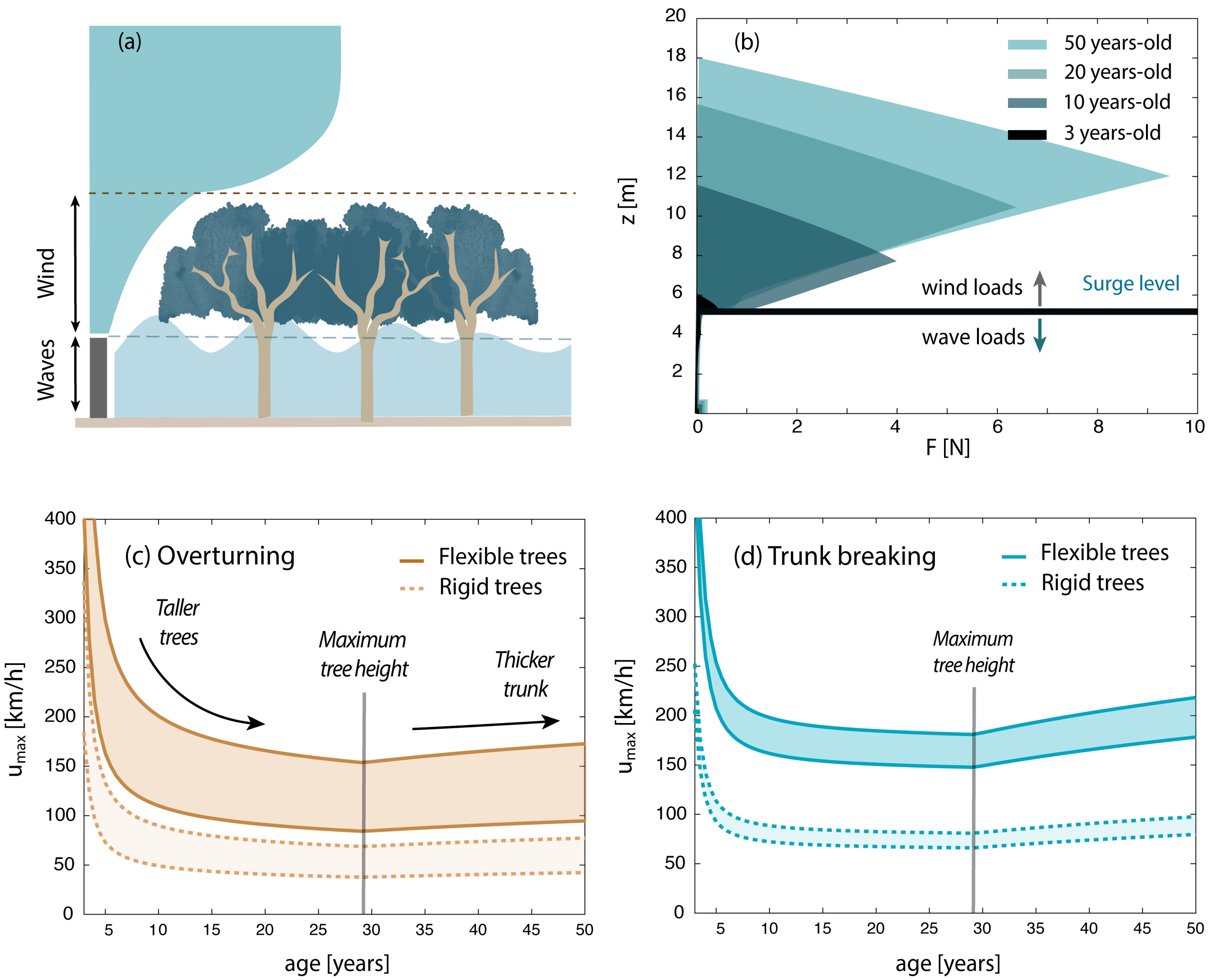

Figure 7. (a) Modelled loads on mangrove trees, consisting of wave loads (on the submerged area) and wind loads (on the emerged area). (b) Modelled forces acting on a mangrove tree placed at the seaward edge of a mangrove belt during a cyclone with wind speeds of 120 km/h. In the model, $c_M = 1$, $c_{D,w} = 2$, $c_{D,c} = 1$, $N_v = 0.1$ trees/m^2, slope = 1/1000, $H_{m0} = 2$ m and $h =$ 5.5 m. (c) Maximum wind speed for overturning as a function of tree age. The results obtained with $c_{D,c} = 0.2$, representing reconfiguration by flexible trees, are shown with solid brown lines, and with $c_{D,c} = 1$, representing rigid trees, in dashed brown lines. The upper and lower lines represent maximum and minimum value of the empirical overturning parameter C_r for terrestrial trees[73]. (d) Maximum wind speed for trunk breaking as a function of tree age. The results obtained with $c_{D,c} = 0.2$, representing flexible trees, are shown with solid blue lines, and with $c_{D,c} = 1$, representing rigid trees, in dashed blue lines. The upper and lower lines represent maximum and minimum value of the modulus of rupture of *S. apetala* trees.[37]

smaller individuals). Nevertheless, after trees reach their maximum height, trunk and branches continue to grow and mangroves slightly increase their stability over time.

The maximum wind speeds that mangroves can withstand depend on whether trees can reduce the loads acting on them by bending. By 30 years old, if trees are fully rigid ($c_{D,c}$ = 1) they can be toppled over by wind speeds between 40-70 km/h, while by being flexible and reducing their frontal area ($c_{D,c}$ = 0.2), they can resist stronger winds up to 80-150 km/h. Drag values oscillated between $c_{D,c}$ = 0.2-1 for western red cedars under winds up to 70 km/h[71], and they are probably on the lower side of this range (or even below it) for mangroves. Cyclones could induce much larger wind speeds than those tested in wind tunnel experiments[71], and *S. apetala* trees have a lower mean modulus of elasticity (2500 N/mm^2)[37] compared to western red cedars (7095 N/mm^2)[85], which suggests that they are more flexible and may deflect even more under extreme conditions. Wind tunnel experiments with mangrove trees are thus recommended to study their motion under strong winds.

Model results suggest that, both with or without flexibility effects, *S. apetala* trees could overturn for sustained wind speeds of 85-260 km/h, which are typical of cyclones in Bangladesh. The threshold wind speeds for trunk breaking are higher than for overturning, indicating that trees are more likely to topple over than to experience stem breaking. However, such results are obtained using values for overturning resistance for terrestrial trees. On the one hand, mangroves are often found muddy sites with soft sediment that could lead to lower C_r values, but on the other hand, they have complex root systems that could provide extra stability compared to terrestrial species. Measuring the stability of *S. apetala* trees is thus recommended to reduce the uncertainty in mangrove stability predictions.

Both forces and tree stability are modelled in a simplified manner, which could be developed in follow-up studies. For instance, dynamic effects in the forces are neglected, and we only model forces experienced at the edge of a forest (without considering sheltering effects between trees). We schematize the overturning strength as a function of the tree weight, but the shape and size of the root system will also influence tree stability[86]. Erosive and accretive processes will also affect the chances of failure, since they can they modify the resisting moment of the tree. Indirect damages as trees fall over neighbouring individuals are also disregarded. Despite the model simplifications, field observations also suggest that mangroves frequently fail during cyclones, and different strategies can be considered to mitigate damages. Smaller trees have been found to be more resistant against failure due to their lower exposure to wind[57], and the relatively shorter pioneer species *Avicennia officinalis* may thus have an advantage during extreme conditions. At managed forests, crown tapering above the design water levels may be a method to prevent mangrove losses[87] while preserving the coastal protection function.

Effect of mangroves on dike design

The embankment height is designed to prevent inundation with total water levels that include surges and wave-run up. Narrow mangrove belts have a very small effect on surges (between 0-0.2 m per km[44]), and the present model thus focuses on how wave reduction by mangroves influences the embankment design. The presence of a mangrove forest has a relatively small effect on embankment crest heights, and, for instance, a 500 m long forest only reduces the required embankment height by 4% (with an age of 50 years old), while increasing the forest width to 1 km long only decreases the maximum height by 5% (Figure 8 a). However, other components of the design are more influenced by wave attenuation - a mangrove belt of 500 m can reduce the revetment thickness by 28% and the bed shear stresses by 63%. An even longer mangrove belt of 1 km would reduce the revetment thickness and shear stresses by 41% and by 83%, respectively. Most of those benefits are already obtained when trees are 10 years old (Figure 8 a-c), due to the fast mangrove growth (Figure 5, c). When the canopy emerges from the water (by approximately 20 years old), the wave attenuation capacity and the effect of mangroves on embankments diminish, but this decrease is compensated by the growth of trunk and roots by the time that trees are 30 years old.

Model results show that the impact of increasing the forest width reduces as the forest becomes longer, since waves attenuate exponentially through the forest[31,88]. However, these results do not include the effect of mangrove failure on wave attenuation predictions. A reduction of the mean tree diameter of 30%, e.g., if the oldest trees collapse during a cyclone and younger trees replace them, would increase wave heights by 20% at the toe of the structure. That increase would imply that the revetment should be 25% thicker or that the forest should be 300 m (60%) longer to compensate for the higher wave exposure (see black arrows in Figure 8 d). It should be noted that fallen trees could still contribute to wave attenuation during the storm event that damaged them, but their effect will disappear over time as they decay.

In this study, we explore the effect of a mangrove belt formed by trees of one species and equal age, but geometry and stability models for more species would be needed to simulate a biodiverse forest. Geometry and growth models could also be expanded to reproduce differences in growth for a single species as a function of site-dependent environmental conditions, and to improve the description of individual trees (e.g., changing the vertical distribution of the surface area with tree age, or including the effect of processes like competition and thinning). With such models, given some general information about the forest population (such as distribution of species and tree ages), it would be possible to calculate the proportion of trees that could be damaged during a storm, and to estimate how wide the forest should be to compensate for tree losses.

Potential damage by pests would also imply that forests may need to be even longer and more biodiverse (containing several

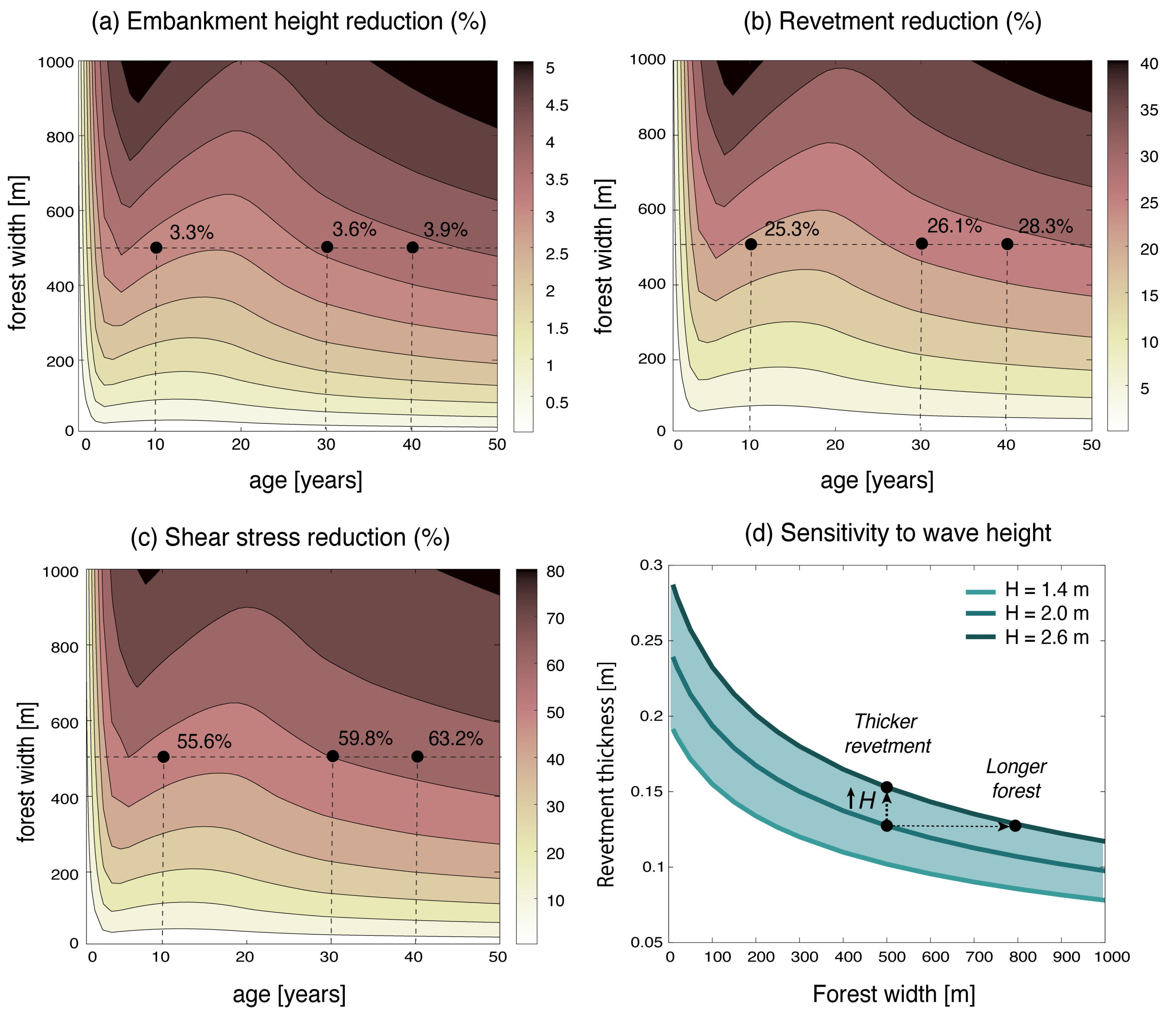

Figure 8. Effect of forest width and age on the reduction of (a) embankment crest height, (b) thickness of the slope protection, and (c) shear stresses at the embankment toe. The bathymetry is assumed linear with a for a bed slope of 1/1000. Vegetation properties in plots (b)-(d) correspond with the tree model presented in Figure 5. In the runs $c_{D,w} = 2$, $N_v = 0.1$ trees/m^2, $H_{m0} = 2$ m and $h = 5$ m at the embankment toe. (d) Sensitivity of the revetment thickness to variations of +/- 20% of the wave height for a tree age of 50-years old.

species) to provide sufficient safety. An additional buffer may also be needed to account for habitat squeezing due to sea level rise. The choice of the optimal mangrove width is therefore site-specific and requires balancing several factors such as the ecological requirements for mangrove establishment and survival, the potential flood risk reduction by the vegetation, and other ecosystem services with the costs and benefits of other land use alternatives. After a target forest width is defined for afforestation, the forest should be monitored and managed over the lifetime of the design, conducting preventive measures before storm or cyclone seasons (like tapering trees) or temporarily reinforcing the embankments while the mangrove forest is recovering from storm damage.

Conclusions

This paper presents a model to evaluate the effect of wave attenuation by mangroves on embankment designs, including tree growth and failure due to winds and waves. The model is applied to potential afforestation sites seawards from coastal embankments in Bangladesh, using the properties of the local mangrove pioneer *Sonneratia apetala*. Model results indicate that wave attenuation predictions are very dependent on the tree surface area. Accurate descriptions of the canopy are necessary for *Sonneratia apetala* trees younger than 20 years old for design water levels of 5 m, whereas the trunk diameter is most important for older trees. Mangrove fringes with cross-shore widths < 1 km have most effect on the slope protection and on the bed erodibility at the embankment toe. However, the effect of wave reduction by such mangrove belts on embankment crest heights is small, since embankment overtopping is dominated by the large surge levels at the potential afforestation sites in Bangladesh. Comparison of overturning moments by winds with the resisting moments of mangroves suggest that *S. apetala* trees could collapse for wind speeds between 85-260 km/h, which are frequently caused by cyclones in Bangladesh. Implementing biodiverse forests with shorter pioneers like *Avicennia officinalis* or tree tapering before cyclone seasons could reduce the chance of tree failure. Post-cyclone field observations and tree pulling experiments would be very valuable to expand the failure mechanisms and develop precise models of mangrove stability. Investigating the changes in mangrove surface area as a function of tree age is also recommended for more accurate wave and wind load predictions. Tree surface area and stability models should also be developed for other mangrove species, in order to facilitate the integration of mangrove forests in coastal protection plans.

Methods

Quantifying mangrove geometry

Predicting wave attenuation by mangroves requires describing their frontal surface area, including roots, trunk, and canopy. A literature study (Figure 1 and Table 1) provides information about the trunk and roots of *S. apetala* mangroves, but no information was found for the canopy. The canopy area is thus obtained by digitizing images of *S. apetala* trees collected in China. The images are scaled assuming a pneumatophore height of 15 cm, which was the average value observed in the area. Overexposure and shadowing resulted in branches and leaves being partly colored and partly black and white, which hinders separating the leave and branch area using color thresholds. Therefore, the contour of the trunk and branches is manually digitized in Photoshop and read as a binary image in MATLAB. Over the height of the tree, the number of pixels corresponding with the tree area are summed to obtain the vertical distribution of the exposed surface. The total tree area is divided by the tree height to calculate an equivalent tree width b_v, which is normalized using the d_{BH} of the tree (b_v/d_{BH}). Since branches with diameters smaller than 1 cm cannot always be identified in the pictures due to inhomogenous lighting, the image analysis focuses on the image with best resolution and colour homogeneity (Figure 9, 1), and the results are compared with a second specimen photographed with less quality (Figure 9, 2). The resulting tree properties are summarized in Table 2.

For the highest quality picture the total tree area (neglecting leaves) is 1.5 m^2 (Figure 9, a), with a diameter at breast height of d_{BH} = 0.13 m and a tree height of h_v = 3.46 m. The canopy starts at h_c = 1 m from the ground, corresponding with 29% of the tree height (h_c = 0.29 h_v), although this value could be underpredicted due to the perspective of the picture. The canopy has a total area of 1.35 m^2 including the trunk, and 1.19 m^2 excluding it. Therefore 90% of the tree frontal area is in the canopy, and 80% in the canopy branches.

Table 2. Tree properties of *Sonneratia apetala* specimens from field pictures, consisting of the tree frontal area A, the diameter at breast height d_{BH}, the vegetation height h_v, the elevation at which the canopy starts compared to the tree height h_c/h_v, and the equivalent width of the tree, $b_v = A/(d_{BH}h_v)$, compared to the diameter at breast height.

Specimen	A [m^2]	d_{BH} [m]	h_v [m]	h_c/h_v [-]	$b_v = A/(h_v d_{BH})$ [m]
Tree 1	1.50	0.13	3.46	0.29	3.0
Tree 1b	0.94	0.13	3.46	0.29	2.1
Tree 2	0.56	0.08	2.62	0.12	2.6

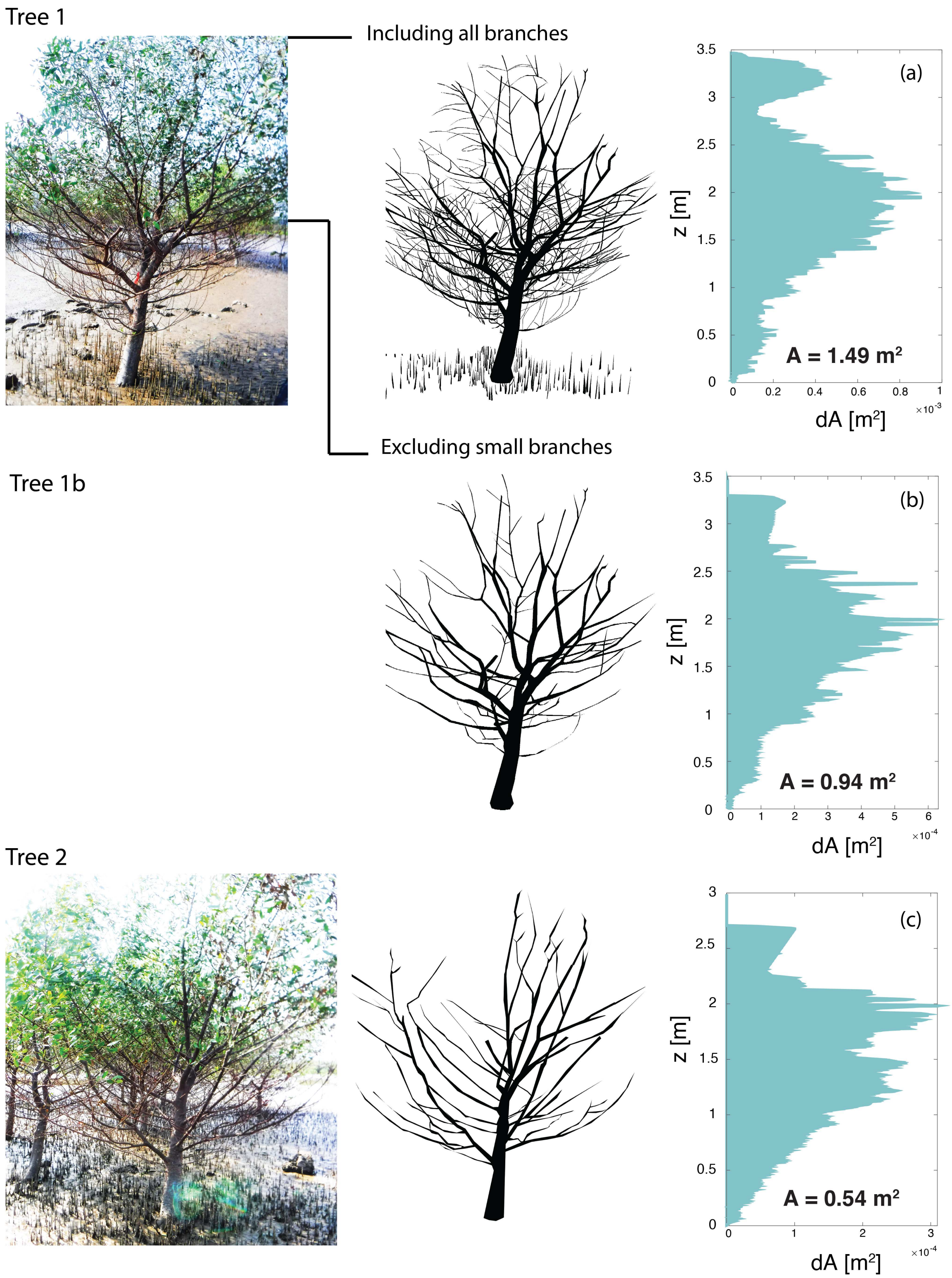

Figure 9. Vertical distribution of the tree area for (a) *S. apetala* tree area of the top left picture (tree 1), of (b) the same tree excluding the smaller branches (tree 1b), and for (c) another *S. apetala* tree from a picture with higher contrast (tree 2), modified from Gijón Mancheño et al.[49]

The size and location of the pneumatophores is distorted, causing an underestimation of the root area at every height. In view of Table 1, assuming a root density of N_r = 100-200 roots/m^2, a root height of $h_r = 0.1$-0.2 m, a root diameter of $d_r = 7$ mm, and that the roots extend over a radius of 2 m from the trunk, the total frontal area of the roots would range between A_c = 0.2-0.9 m^2, which would increase the tree frontal area in 30-60% with respect to the estimates of Table 2. Removing the the branches smaller than 1 cm and the pneumatophores (Figure 9, b) reduces the total tree area from $A = 1.5$ m^2 to A = 0.94 m^2 (in 37%).

A second *S. apetala* specimen where the smallest branches are not distinguisible due to lower image quality (Figure 9, 2) has a total area of $A = 0.56$ m^2 (Figure 9, c), a diameter at breast height of d_{BH} = 0.08 m, and a tree height of h_v = 2.62 m. For the second specimen, the canopy starts at $h_c = 0.32$ m above the ground, corresponding with 12% of the tree height ($h_c = 0.12h_v$). The vertical distribution of the tree areas shows a maximum at the canopy, even neglecting the leaves and the smallest branches. In this analysis, small branches are neglected and leaves are also disregarded under the assumption that they are quite flexible and easily detachable[37]. Despite their flexibility, these elements likely contribute to some extent to wave dissipation by the trees.

Relationships for mangrove growth

For a given tree age, the height h_v and trunk diameter d_{BH} are obtained from a fit to the data of *S. apetala* trees from Bangladesh shown in Figure 1. The equivalent tree width is obtained by multiplying the normalized b_v value by the d_{BH}. The evolution of the tree structure as a function of age is obtained combining the growth relationships from Figure 1 with the vertical distribution of the tree area from the field images.

Since the scaling is approximated and the images are not corrected to account for the perspective, the areas and equivalent widths obtained from the field pictures are only an approximation, and should be investigated in follow up field studies. However, they provide an indication on the vertical distribution of the frontal surface, and how the canopy area compares to the area of the trunk.

The vertical structure of the mangrove trees is schematized by combining information from the literature (Table 1) and from the analysis of field pictures (Figure 9). Three tree sections are considered: roots, trunk, and canopy (Figure 5, a). The root height is assumed to correspond with 4% of the tree height (h_r = 0.04 h_v), and the total root width (adding the width of all the pneumatophores), is set equal to 12 times the diameter at breast height (b_r = 12 d_{BH}). The canopy is assumed to start at 33% of the tree height ($h_c = 0.33\ h_v$). Considering a total canopy area equal to A_c = 3 $d_{BH}h_v$, a trapezoidal canopy with the same area would have a maximum width of $b_{v,max} = 7d_{BH}$. The resulting tree structure as a function of the distance from the ground is shown in Figure 5 (b). The evolution of the tree structure as a function of age is shown in Figure 5 (c).

Data availability

The datasets used and/or analysed during the current study available from the corresponding author on reasonable request.

References

1. McIvor, A., Möller, I., Spencer, T. & Spalding, M. Reduction of wind and swell waves by mangroves. natural coastal protection series: Report 1. Tech. Rep., Cambridge coastal research unit working paper 40. The nature conservancy, Arlington, USA/Wetlands International, Wageningen, Netherlands, pp 27 (2012).
2. Menéndez, P., Losada, I., Torres-Ortega, S., Narayan, S. & Beck, M. The Global Flood Protection Benefits of Mangroves. *Sci. Reports* **1** (2020).
3. van Zelst, V., Dijkstra, J., van Wesenbeeck, B. & et al. Cutting the costs of coastal protection by integrating vegetation in flood defences. *Nat Commun* **12** (2021).
4. Tiggeloven, T. *et al.* The benefits of coastal adaptation through conservation of foreshore vegetation. *J. Flood Risk Manag.* **15**, DOI: https://doi.org/10.1016/j.jseaes.2006.05.011 (2022). Morphodynamics of the Red River Delta, Vietnam.
5. Brander, L. *et al.* Ecosystem service values for mangroves in Southeast Asia: A meta-analysis and value transfer application. *Ecosyst. services* **1** (2012).
6. Woodroffe, C., Rogers, K., McKee, K., Lovelock, I., C.E.and Mendelssohn & Saintilan, N. Mangrove Sedimentation and Response to Relative Sea-Level Rise. *Annu. Rev. Mar. Sci.* **8** (2016).
7. Lovelock, C. *et al.* The vulnerability of Indo-Pacific mangrove forests to sea-level rise. *Nature* **526** (2015).
8. Saintilan, N. *et al.* Thresholds of mangrove survival under rapid sea level rise. *Science* **368** (2020).
9. Murdiyarso, D. *et al.* The potential of Indonesian mangrove forests for global climate change mitigation. *Nat. Clim. Chang.* **5** (2015).

10. Srikanth, S., Lum, S. & Chen, Z. Mangrove root: adaptations and ecological importance. *Trees* **30** (2016).

11. Snedaker, S. Mangrove species zonation: why? *Contributions to Ecol. Halophytes. Springer, Dordrecht* (1982).

12. Ellison, A., Mukherjee, B. & Karim, A. Testing patterns of zonation in mangroves: scale dependence and environmental correlates in the Sundarbans of Bangladesh. *J. Ecol.* **88** (2000).

13. Bunt, J. Mangrove zonation: An examination of data from seventeen riverine estuaries in tropical australia. *Annals Bot.* **78** (1996).

14. Lopez-Portillo, J. & Ezcurra, E. Zonation in mangrove and salt marsh vegetation at laguna de mecoacan, mexico. *Biotropica* **21** (1981).

15. Carrol, C., Bunting, P., Hardy, A. & Bell, G. Using continuous change detection and classification of landsat data to investigate long-term mangrove dynamics in the sundarbans region. *Remote. Sens.* **11** (2019).

16. Bhowmik, A. & Cabral, P. Cyclone sidr impacts on the sundarbans floristic diversity. *Earth Sci. Res.* **2** (2013).

17. Eckstein, D., Künzel, V., Schäfer, L. & Winges, M. Global Climate Risk Index 2019. *Ger. e.V.* (2020).

18. Saenger, P. & Siddiqi, N. Land from the sea: The mangrove afforestation program of Bangladesh. *Ocean. Coast. Manag.* **20**, 23–39 (1993).

19. Gijón Mancheño, A. *et al.* Mapping mangrove opportunities with open access data: A case study for bangladesh. *Sustainability* **13** (2021).

20. Jakobsen, F., Zeaul Hoque, A., Paudyal, G. & Bhuiyan, M. S. Bringing in the tides. From closing down to opening up delta polders via Tidal River Management in the southwest delta of Bangladesh. *Water Policy* **19**, 147–164 (2017).

21. Vuik, V., Jonkman, S., Borsje, B., & Suzuki, T. Nature-based flood protection: The efficiency of vegetated foreshores for reducing wave loads on coastal dikes. *Coast. Eng.* **116** (2016).

22. Vuik, V. *et al.* Assessing safety of nature-based flood defenses: Dealing with extremes and uncertainties. *Coast. Eng.* **39** (2018).

23. Vuik, V., Borsje, B., Willemsen, P. & Jonkman, S. Salt marshes for flood risk reduction: Quantifying long-term effectiveness and life-cycle costs. *Ocean. Coast. Manag.* **171** (2019).

24. Rahman, M., , Zimmer, M. & Ahmed, I. Co-benefits of protecting mangroves for biodiversity conservation and carbon storage. *Nat Commun* **12** (2021).

25. Wang, Q. *et al.* Sequestration of heavy metal by glomalin-related soil protein: Implication for water quality improvement in mangrove wetlands. *Water Res.* **148** (2019).

26. Montgomery, J., Bryan, K., Horstman, E. & Mullarney, J. Attenuation of Tides and Surges by Mangroves: Contrasting Case Studies from New Zealand. *Water* **10** (2018).

27. Krauss, K. *et al.* Water level observations in mangrove swamps during two hurricanes in Florida. *Wetlands* **29**, 142–149 (2009).

28. Dasgupta, S. *et al.* Vulnerability of bangladesh to cyclones in a changing climate: Potential damages and adaptation costs. Tech. Rep., Policy Research Working aper 5280, The World Bank Development Research Group, Environment and Energy Team (2010).

29. Mazda, Y., Wolanski, E. & King, B. Drag force due to vegetation in mangrove swamps. . *Mangroves Salt Marshes* **1**, 193–199 (1997).

30. Quartel, S., Kroon, A., Augustinus, P., Van Santen, P. & Tri, N. Wave attenuation in coastal mangroves in the red river delta, Vietnam. *J. Asian Earth Sci.* **29**, 576–584 (2007).

31. Bao, T. Effect of mangrove forest structures on wave attenuation in coastal Vietnam. *Oceanologia* **53** (2011).

32. Horstman, E. *et al.* Wave attenuation in mangroves: A quantitative approach to field observations. *Coast. Eng.* **94**, 47–62 (2014).

33. Méndez, F. & Losada, I. An empirical model to estimate the propagation of random breaking and nonbreaking waves over vegetation fields. *Coast. Eng.* **51**, 103–118 (2004).

34. Uddin, M. & Hossain, M. Growth performance of coastal plantations and land stabilization in an offshore island of hatiya, noakhali, bangladesh. *Bangladesh J. For. Sci.* **32** (2013).

35. Islam, S., Miah, S., Habib, M. & Alam, M. Growth and yield of sonneratia apetala (keora) plantations raised from different seed sources in the central coastal belt of bangladesh. *J. Biosci. Agric. Res.* **6** (2016).

36. Quine, P. & Gardiner, B. Understanding how the interaction of wind and trees results in windthrow, stem breakage and canopy gap formation. draft of 2/08/05. *Plant Disturb. Ecol.* (2007).

37. Van Hespen, R. *et al.* Analysis of coastal storm damage resistance in successional mangrove species. *Limnol. Oceanogr.* **1999** (2021).

38. Van der Meer, J. *et al.* Manual on wave overtopping of sea defences and related structures. Tech. Rep., An overtopping manual largely based on European resreach, but for worldwide application. www.overtopping-manual.com: EurOtop (2018).

39. Pilarczyk, K. Coastal protection. *A.A. Balkema, Rotterdam* (1990).

40. Pilarczyk, K. Dikes and revetments. *A.A. Balkema, Rotterdam* (1998).

41. Wang, W., Li, X. & Wang, M. Propagule dispersal determines mangrove zonation at intertidal and estuarine scales. *Forests* **10** (2019).

42. Snedaker, S. Mangrove species zonation: Why? *Tasks for Veg. Sci.* **2** (1982).

43. Maza, M., Lara, J. & Losada, I. Predicting the evolution of coastal protection service with mangrove forest age. *Coast. Eng.* **168** (2021).

44. Krauss, K. *et al.* Environmental drivers in mangrove establishment and early development: A review. *Aquatic Bot.* **89** (2008).

45. Rahman, M., Sass-Klaassen, U., Zuidema, P., Chowdhury, M. & Beeckman, H. Salinity drives growth dynamics of the mangrove tree sonneratia apetala in the sundarbans, bangladesh. *Dendrochronologia* **12** (2020).

46. Simard, M., Fatoyinbo, L. & Smetanka, C. e. a. Mangrove canopy height globally related to precipitation, temperature and cyclone frequency. *Nat. Geosci.* **12** (2019).

47. Wang, G., Zhang, Y., Guan, D., Xiao, L. & Singh, M. The potential of mature sonneratia apetala plantations to enhance carbon stocks in the zhanjiang mangrove national nature reserve. *Ecol. Indic.* **133** (2021).

48. Xin, K., Zhou, Q., Arndt, S., & Yang, X. Invasive capacity of the manrgove sonneratia apetala in hainan island, china. *J. Trop. For. Sci.* **25** (2013).

49. Gijón Mancheño, A. *et al.* Wave reduction by mangroves during cyclones in bangladesh. Tech. Rep., Policy Research Working Paper 10240 (2021).

50. Zhang, Y. *et al.* Non-linear wave attenuation quantification model improves the estimation of wave attenuation efficiency of mangroves. *Estuarine, Coast. Shelf Sci.* **245** (2021).

51. Suzuki, T., Zijlema, M., Burger, B., Meijer, M. & Narayan, S. Wave dissipation by vegetation with layer schematization in SWAN. *Coast. Eng.* **59**, 64–71 (2012).

52. Massel, S., Furukawa, K. & Brinkman, R. Surface wave propagation in mangrove forests. *Fluid Dyn. Res.* **24** (1999).

53. Van Wesenbeeck, B. *et al.* Wave attenuation through forests under extreme conditions. *Sci. Reports* **12** (2022).

54. Kalloe, S., Hofland, B., Antolínez, J. & van Wesenbeeck, B. Quantifying frontal- surface area of woody vegetation: A crucial parameter for wave attenuation. *Front. Mar. Sci.* **23** (2022).

55. Lopez-Portillo, J., Lewis III, R., Saenger, P. & Rovai, A. *Mangrove Forest Restoration and Rehabilitation. Mangrove Ecosystems: A Global Biogeographic Perspective* (Springer, Cham., 2017).

56. Myers, R. & van Lear, D. Hurricane–fire interactions in coastal forests of the south: a review and hypothesis. *For. Ecol. Manag.* **103** (1998).

57. Krauss, K. & Osland, M. Tropical cyclones and the organization of mangrove forests: a review. *Annals Bot.* **125** (2020).

58. Herrera-Silveira, J. A. *et al.* Hurricane damages to mangrove forests and post-storm restoration techniques and costs. *The Nat. Conserv. Arlington, VA* (2022).

59. Mandal, M. & Hosaka, T. Assessing cyclone disturbances (1988–2016) in the sundarbans mangrove forests using landsat and google earth engine. *Nat Hazards* **102** (2020).

60. Dutta, D., Das, P., Paul, S., Sharma, R. & Dadhwal, V. Hassessment of ecological disturbance in the mangrove forest of sundarbans caused by cyclones using modis time-series data (2001–2011). *Nat Hazards* **79** (2015).

61. Pendleton, L. *et al.* Estimating global “blue carbon” emissions from conversion and degradation of vegetated coastal ecosystems. *PLoS ONE* **7** (2012).

62. Gardiner, B., Berry, P. & Moulia, B. Review: Wind impacts on plant growth, mechanics and damage. *Plant Sci.* **245** (2016).

63. Rahman, M., Donoghue, D., Bracken, L. & Mahmood, H. Biomass estimation in mangrove forests: a comparison of allometric models incorporating species and structural information. *Environ. Res. Lett.* **16** (2021).

64. Karim, M. & N., M. Impacts of climate change and sea-level rise on cyclonic storm surge floods in Bangladesh. *Glob. Environ. Chang.* **18**, 490–500 (2008).

65. Zaman, S. & Mondal, M. Risk-based determination of polder height against storm surge Hazard in the south-west coastal area of Bangladesh. *Prog. Disaster Sci.* **8** (2020).

66. Balke, T. *et al.* Windows of opportunity: Thresholds to mangrove seedling establishment on tidal flats. *Mar. Ecol. Prog. Ser.* **440** (2011).

67. Mo, Y., Simard, M. & Hall, J. Tropical cyclone risk to global mangrove ecosystems: potential future regional shifts. *Front. Ecol. Environ.* (2023).

68. Thornton, E. & Guza, R. Transformation of wave height distribution. *J. Geophys. Res.* **88** (1983).

69. Morison, J. R., O'Brien, M. P., Johnson, J. W. & Schaaf, S. A. The force exerted by surface waves on piles. *Petroleum Trans.* **189**, 149–157 (1950).

70. Gijón Mancheño, A. *et al.* Wave transmission and drag coefficients through dense cylinder arrays: implications for designing nature-based structures. *Ecol. Eng.* **165** (2021).

71. Rudnicki, M., Mitchell, S. & Novak, M. Wind tunnel measurements of crown streamlining and drag relationships for three conifer species. *Can. J. For. Res.* **34** (2004).

72. Bardal, L. & Saetran, L. Wind gust factors in a coastal wind climate. *Energy Procedia* **94** (2016).

73. Nicoll, B., Gardiner, B., Rayner, B. & Peace, A. Anchorage of coniferous trees in relation to species soil type, and rooting depth,. *Can. J. For. Res.* **36** (2016).

74. Khan, Z. Disaster impact on sundarbans: A case study on sidr affected area. *IMPACT: Int. J. Res. Applied, Nat. Soc. Sci.* (2016).

75. Ghosh, M., Kumar, L. & Langat, P. Geospatial modelling of the inundation levels in the sundarbans mangrove forests due to the impact of sea level rise and identification of affected species and regions. *Geomatics, Nat. Hazards Risk* **10** (2019).

76. Tanaka, N. Investigation team of japan society of civil engineering. investigation report on the stormsurge disaster by cyclone sidr in 2007, bangladesh. Tech. Rep., JSCE (2011).

77. Hussain, M., Tajima, Y., Hossain, M. & Das., P. Impact of cyclone track features and tidal phase shift upon surge characteristics in the bay of bengal along the bangladesh coast. *J. Mar. Sci. Eng.* **5** (2017).

78. Haque, A., Kay, S. & Nicholls, R. Present and future fluvial, tidal and storm surge flooding in coastal bangladesh. *Ecosyst. Serv. for Well-Being Deltas* (2018).

79. Zhang, X., Lin, P. & Chen, X. Coastal protection by planted mangrove forest during typhoon mangkhut. *J. Mar. Sci. Eng.* **10** (2022).

80. Zhu, D., Hui, D. & Wang, M. e. a. Allometric growth and carbon storage in the mangrove sonneratia apetala. *Wetl. Ecol Manag.* **29** (2021).

81. Peterson, T. & Cannon, J. Modelling wind damage to southeastern u.s. trees: Effects of wind profile, gaps, neighborhood interactions, and wind direction. *Front. For. Glob. Chang.* **4** (2021).

82. *D-Morphology User Manual. Version 2023 of 8th December 2022*.

83. IWM. Technical report on storm surge, wave, hydrodynamic modelling and design parameters on drainage system and embankment crest level. volume-ii: Package 2 (appendix-b: Storm surge). Tech. Rep., Bangladesh Water Development Board, Ministry of Water Resources (2018).

84. of Bangladesh, G. Detailed design of five polders. volume i: Design report. Tech. Rep., Government of Bangladesh (2012).

85. Molinkski, W., Mania, P. & Tomczuk, G. The usefulness of different wood species for bow manufacturing. *Folia For. Polonica* **58** (2016).

86. van Hespen, R. *Establishment and survival of coastal mangrove trees under mechanical disturbances*. Ph.D. thesis, University of Utrecht (2023).

87. Halder, N., Merchant, A., Misbahuzzaman, K., Wagner, S. & Mukul, S. Why some trees are more vulnerable during catastrophic cyclone events in the sundarbans mangrove forest of bangladesh? *For. Ecol. Manag.* **490** (2021).

88. Dalrymple, R., Kirby, J. & Hwang, P. Wave Diffraction Due to Areas of Energy Dissipation. *J. Waterw. Port, Coast. Ocean. Eng.* **110**, 67–79 (1984).

Acknowledgements

This paper is based on the World Bank Policy Report 10240, undertaken at Delft University of Technology within the contract number 7204185. The research was funded by a grant received by the World Bank through the European Union and managed by GFDRR. The authors would like to thank the World Bank peer reviewers for their comments.

Author contributions statement

A.G.M. developed the model, R.v.H. collected the field images, V.V., B.K.W. and S.N.J. contributed to the results interpretation and draft writing, R.M., S.K., I.U. and M.L. contributed to the writing and reviewing of this work.

Additional information

The authors declare no competing interests.